RESPONSE OF COMPOSITE PLATES

SUBJECTED TO ACOUSTIC LOADING

By: E. Thomas Moyer Jr.

Associate Professor of Engineering and Applied Science

The George Washington University

Final Technical Report For NASA Grant #NAG 1-158

Technical Monitors:

Dr. John Mixson

Mr. Carl Rucker

January, 1989

INTRODUCTION

The objectives of NASA Grant #NAG-1-158, "Response of Composite Plates Subjected to Acoustic Loading" were to investigate numerical methodology for the determination of narrowband response in the geometrically nonlinear regime, to determine response characteristics for geometrically nonlinear plates subjected to random loading and to compare the predictions with experiments to be performed at NASA Langley Research Center. The first two objectives were met. The response of composite plates subjected to both narrowband and broadband excitation have been studied and much useful information has been obtained (as will be discussed in this report and is documented in two AIAA papers [1,2]). The third objective could not be met due to lack of experimental success and the decision to discontinue this research on the part of the sponsors. A brief summary of the experimental efforts can be found in Appendix A of this report.

The problem of determining the response of composite panels subjected to high intensity acoustic loading is of extreme importance for future flight applications involving high speed, high altitude flight of structures which contain composite members. Several reports and papers have indicated that future flight applications are likely to require composite panels to perform under acoustic loading conditions which will produce geometrically

nonlinear responses [3,4,5]. Even though the application is crucial, little robust analysis methodology exists which can determine the response characteristics in this regime. This report addresses a methodology approach which can handle a wide variety of applications in a robust, self consistent manner.

The problem of the geometrically nonlinear response of composite panels subjected to narrowband, sinusoidal loading was studied initially. It is well known that flat plates exhibit response characteristics which are multivalued in the frequency domain. This phenomena manifests itself in jump characteristics which can be observed experimentally. A numerical approach to the solution of this problem was developed and reported previously [1]. This work demonstrated that a time domain integration approach with a phased damping model and an energy convergence criterion could predict the solution quite accurately. In addition, a numerical method was proposed and tested for the prediction of jump phenomena. This approach did not require the advocation of an ad hoc stability criteria. As was expected, the differential equation contained all relevant information for the prediction of the jump frequencies. It was demonstrated that the nonphysical solution was numerically unstable. The typical hard spring response was accurately predicted and the metastable transition response characteristics were predicted. This paper is contained in Appendix B which details this work.

The problem of the response of a composite plate subjected to

random loading was studied next. Several different approaches have been proposed over the years for the analysis of nonlinear systems subjected to random time histories. These include exact (Fokker-Planck) equation solutions [6,7], perturbation approaches [8,9], stochastic linearization [10,11] and time domain (or Monte Carlo) approaches [12,13]. The Fokker-Planck equation solutions and perturbation approaches are discussed in the referenced literature. Neither methodology, however, can be employed for general loading and arbitrary degrees of nonlinearity. These approaches, therefore, were not pursued.

The method of stochastic linearization is based on the assumption of a known response density function. While most authors employ a Gaussian closure, current work is focusing on non-Gaussian closures. The basic approach seeks an approximate solution to the nonlinear problem by proposing a "equivalent" linear problem which exhibits similar response statistics. While this method is analytically attractive since the solution of the equivalent linear system is trivial, it requires knowledge of the response density function and can only minimize error with respect to a few response statistics (most commonly the RMS response). As is shown in [2], stochastic linearization produces good results for the response statistics for which the error is minimized but does not predict the correct spectral characteristics. In addition, the approach assumes that the spectral response width is independent of the nonlinearity (the peak response frequency, however, is dependent on the nonlinearity) which is demonstrated to be incorrect.

The time domain or Monte Carlo simulation approach appears to be the most rigorous and robust approach to the solution of the problem of determining the response characteristics of a composite plate undergoing geometrically large deflections due to random excitation. This approach was compared with the method of stochastic linearization and with the exact solution for white noise excitation in [2]. The exact response density function and response statistics were predicted by the time domain simulation method. Much discrepancy exists, however, between the exact (and numerical time domain) solution and the stochastic linearization solution. The details from [2] are given in Appendix C.

This report will discuss the results obtained from varying the degree of geometric nonlinearity, damping and loading amplitude. Special focus is placed on the characteristics and coupling of these effects. All solutions were generated for white noise loading (where the numerically predicted response density matches the exact solution) and clamped boundary condition (which cause the most severe response and fatigue characteristics).

TIME DOMAIN SIMULATION APPROACH

For a composite panel subjected to a uniform pressure loading with

random time history, the single mode response reduces the governing system to the well known Duffing equation given by

$$\frac{d^2\varphi}{dt^2} + 2 \zeta \omega \frac{d\varphi}{dt} + \omega^2\varphi + \lambda\beta\varphi^3 = F(t)$$

where

ω => Linear Resonance Frequency

φ => Response Function

ζ => Damping Factor

β => Hard Spring Coefficient

λ => Nonlinearity Parameter

$F(t)$ => Forcing Function

For comparative purposes, the hard spring coefficient was taken for the composite panel discussed in Appendix C. The nonlinearity parameter was varied to study the effects of increased and decreased nonlinearity. A value of unity corresponds to the results in Appendix C. In addition, soft spring characteristics could be studied by employing negative nonlinearity parameters.

The Duffing equation was integrated using the implicit Newmark integrator as discussed in Appendix C. During the course of this research, several integrators were investigated: explicit second order central differences, explicit Runge-Kutta algorithms (both fourth and sixth order) and two of the implicit Gear integrators (specially designed for stiff systems). These algorithms are

detailed in numerical analysis text books (e.g. [14]) and will not be repeated here.

Integration with explicit algorithms was unsuccessful. The time step size had to be chosen prohibitively small to accommodate random loading and maintain stability. Adaptive measures appear to be promising, however, due to the nonlinearity, they must be developed empirically and would depend on all involved parameters. This approach was demonstrated for one response but was still computationally expensive compared with the Newmark approach. Increasing the order of the integrator did not improve the situation as the required time step size was governed by stability and not accuracy. The stable time step size appeared to produce response statistics and response density functions which were within 1% of the exact solution. Explicit integration was not pursued further.

The Gear integrators were tested on the problem also. These integrators were developed for integration of stiff equations (mainly for application in the field of chemical kinetics). For first order stiff systems (which exhibit exponential characteristics), these integrators have been very successful. For problems with time harmonic characteristics (such as vibration problems), they have not been very successful. Both second and fourth order Gear integrators were tried for three of the parameter sets studied. The convergent time step size was much smaller (approximately 20%) than required by the Newmark integrator. In

addition, the resulting nonlinear algebraic equation was more difficult to solve using Newton's method. This was especially true for balanced nonlinearity (where the linear and RMS nonlinear stiffness were approximately equal). The time step had to be reduced almost an order of magnitude before Newton's method would converge from time step to time step. The Gear integrators, therefore, were abandoned.

The Newmark integrator proved to be a stable and accurate performer for this application. The convergence and staggered damping algorithm employed are discussed in Appendix C. The convergence characteristics seemed quite insensitive to the degree of nonlinearity and damping (for the range studied). The adaptive time stepping discussed in Appendix C was also quite insensitive to changes in damping and nonlinearity. Since this algorithm was developed empirically, a more optimal approach should be pursued for application to regimes with significantly different characteristics. The parameters chosen produced the exact response density (within 1%) for the most severe cases (e.g. highest degree of nonlinearity, both extremes in damping and highest RMS response).

To investigate the effects of varying nonlinearity and damping, the time histories were generated by integrating the Duffing equation to a steady state and continuing until 1,000,000 samples were obtained (as detailed in Appendix C). The RMS response was calculated for each case as well as the response spectral density

(often called the Power Spectral Density or PSD). Since the response density was symmetric, only even statistical moments contain useful information for white noise loading. For other loading distributions, however, odd order statistical moments may prove informative. Due to time limitations, only the RMS moment was analyzed. This is further discussed in the last section.

A modified algorithm for Spectral Density estimation was introduced to improve the accuracy of the calculation. An overlapping window approach was employed which minimized variance significantly. For linear problems where the exact PSD is known, the overlapping approach reduced variance by almost an order of magnitude. Details of this algorithm are given in Appendix C. This approach was employed for all results to be presented.

RESULTS AND DISCUSSION

For the purposes of this study, three different nonlinearity parameters (λ = 0.5, 1.0, 1.5) , five different damping factors (ζ = 0.02 , 0.04 , 0.06 , 0.08 , 0.10) and six different excitation amplitudes (70, 80, 90, 100, 110, 120 dB) were investigated. For each combination of the parameters, the RMS response amplitude and Response Spectral Density (RSD) were calculated. As previously discussed, the response density function is non-Gaussian and known for this special case of white noise (see Appendix C).

For the nonlinearity parameter of 0.5 (the least nonlinearity studied), the RMS response is shown in Figure 1. For all damping levels studied (up to 10% of critical), the nonlinearity is evident in the RMS response by 110 dB loading level. At the low end of the damping, nonlinearity is evident at 100 dB. Though not evident on the logarithmic scale, there is measurable (greater than 10%) deviation from linearity at 90 dB.

Figures 2 and 3 show the RMS response for the nonlinearity parameter equal to 1.0 and 1.5 . At 1.0, the deviation from the linear RMS curve is larger than at 0.5. This is the expected result for increasing nonlinearity. It is interesting to note that even for loading levels of 90 dB (which is not terribly severe), this typical panel (described in Appendix C) demonstrates nonlinearity which should not be ignored. As will be evident subsequently, this effect can be seen more clearly in the shift of the spectral peaks. At a nonlinearity parameter of 1.5, the nonlinearity is evident on the plot at 100 dB. Since the increased nonlinearity also increases the stiffness of the plate, the amplitude is lower and, therefore, the deviation from the linear line is less. This is not to be confused with a lesser degree of nonlinearity.

Figures 4, 5 and 6 show the RMS response at constant damping factors of 0.02, 0.06 and 0.10 as a function of the nonlinearity parameter. The larger amplitude is predicted at the lower

nonlinearity parameter since the total stiffness is a monotonically increasing function of the nonlinearity parameter. As the damping level increases, the nonlinearity parameter is not as critical a factor as the increased damping diminishes the RMS response and hence the nonlinear stiffness contribution. As is evident in Figure 6, even at a large damping ratio of 10% critical, nonlinearity is evident (even on a logarithmic scale) at 100 dB which may be evident in many applications.

Figure 7 shows the RSD as a function of loading amplitude for a constant damping ratio of 2% critical and a nonlinearity parameter of 1.0 . As the amplitude increases, the spectral peak near the linear resonance frequency shifts to a larger frequency which is typical of a hard spring nonlinear response. For a loading level of 90 dB, the peak has shifted on the order of 10%. It is interesting to note that as the peak shifts, it also broadens. Spectral broadening has been noticed experimentally by several researchers (as discussed in Appendix C). Often, spectral broadening is attributed solely to damping phenomena (often modeled as nonlinear damping effects). Nonlinear stiffness effects have not been considered a mechanism for spectral broadening previously.

Figures 8 and 9 show the RSD at nonlinearity parameter values of 0.5 and 1.5 . For the smaller nonlinearity parameter, the RSD is larger than for the higher values. This is due to the fact that increased nonlinearity parameter increases the total stiffness of the oscillator. Increased stiffness decreases the response,

suppressing the RSD. Each of these plots demonstrates shifting of the spectral peaks for loading levels of 90 dB and larger. It is interesting to note, that for a loading level of 120 dB, no peaks of any form can be discerned. The RSD exhibits a gradual rise from the zero frequency value over the range plotted. If the calculation were performed to higher frequencies, the RSD is expected to gradually decrease past a limiting value of frequency. The numerical results generated are valid out to a frequency of 1000 hz. The RSD calculations are valid out to 500 hz. This phenomena was not investigated further in this study.

Figures 10, 11, 12 and 13 show the RSD at a fixed value of the nonlinearity parameter (1.0) and damping levels of 4%, 6%, 8% and 10% of critical (respectively). As the damping increases, more spectral broadening is observed. In addition, the peaks shift less at higher damping levels. As damping increases, the spectral broadening due to damping is evidenced at low loading levels. At high loading levels, however, due to the decreased nonlinear stiffness term, the total spectral broadening decreases due to the decreased nonlinear stiffness and, therefore, decreased broadening due to nonlinear stiffness (this will be more evident when the data is shown at constant amplitude and nonlinearity parameter).

Figures 14 and 15 show the RSD for a damping level of 10% critical with nonlinearity parameters of 0.5 and 1.5. For increased nonlinearity parameter, the peaks broaden due the increased nonlinear stiffness. Even though the response amplitude is

decreased at the larger nonlinearity parameter (due to the larger total stiffness), the spectral broadening is greater. This would suggest that the percentage of stiffness due to the nonlinear term is a governing parameter for the degree of spectral broadening.

Figures 16 and 17 show the RSD predicted for a nonlinearity parameter of 1.0 and a driving amplitude of 70 and 80 dB. As expected, the response is linear. At larger damping ratios the peak broadens, however, the frequency of maximum RSD remains the same (i.e. no spectral shift is observed). Figures 18 and 19 show the RSD at a driving amplitude of 80 dB for nonlinearity parameters of 0.5 and 1.5 . As expected, since the response is linear at this point, little difference is observed.

Figures 20, 21 and 22 show the RSD at 90, 100 and 110 dB with the nonlinearity parameter equal to 1.0 . As the amplitude increases, the peaks shift and broaden at all damping levels. It is clearly evident in Figures 21 and 22 that less peak shift and less peak shift is evident at higher damping levels. In other words, at a constant amplitude and nonlinearity parameter, the spectral peaks get narrower at higher damping levels since the additional damping decreases the amplitude which decreases the nonlinear stiffness and decreases the spectral broadening due to nonlinear stiffness effects.

Figures 23 and 24 show the RSD at 110 dB for nonlinearity parameters of 0.5 and 1.5. All exhibit the same decrease in

spectral width with increasing damping. It is dramatically demonstrated in Figure 24. Figure 25 shows the RSD at 120 dB for the nonlinearity parameter equal to 1.0 . For large damping, a round, broad peak region can be identified. As the damping decreases, however, the peak broadens to the point of losing distinction. At large amplitude loading, the RSD exhibits wide, flat spectral characteristics.

Figure 26 shows the RSD at 90 dB with 2% critical damping as a function of the nonlinearity parameter. As mentioned previously, the larger nonlinearity parameter shifts the peak to a greater degree than for smaller nonlinearity parameters. This is slightly evident in Figure 26. For the same amplitude, Figures 27 and 28 show the RSD for 6% and 10% critical damping levels. The increased damping suppresses the response and lessens the nonlinear stiffness effects. At these damping levels, therefore, the effect of the nonlinearity parameter is minimal.

Figure 29 shows the RSD at a loading amplitude of 100 dB and a damping level of 6% critical. While not evident at 90 dB, the nonlinear stiffness parameter shifts, broadens and flattens the peak some at 100 dB for this damping level. Figure 30 shows the RSD at 100 dB for 10% critical damping. There is still little influence due to the nonlinearity parameter under these conditions.

Figure 31 shows the RSD at 110 dB with 2% critical damping.

Increasing the nonlinearity parameter significantly shifts, broadens and flattens the RSD under these conditions. Figures 32 and 33 show the RSD at 110 dB for 6% and 10% critical damping. While the nonlinearity parameter shifts broadens and flattens the response in these figures also, the degree is diminished as a function of increased damping. At 110 dB with 10% critical damping, the spectral widths, while showing some broadening due to nonlinearity parameter, are not very dramatically changed. This indicates that there may be a crossover point (for constant amplitude loading) where the damping ceases to dominate the spectral width and where the nonlinear stiffness effects become the dominant broadening mechanism.

CONCLUDING REMARKS

The work under NASA Grant #NAG 1-158, "Response of Composite Plates Subjected to Acoustic Loading" produced many significant and insightful results which should enhance the understanding of randomly excited nonlinear oscillators and, ultimately, lead to accurate prediction of sonic fatigue characteristics. During the two funded years of this research grant (and the six month no cost extension), two papers were presented and published with the AIAA. In addition, a third paper incorporating all the results presented in this report is under preparation for submission to an appropriate journal. Upon completion, this paper will be forwarded to the NASA Grant Monitors, Dr. John Mixson and Mr. Carl Rucker.

The results of this research demonstrated that nonlinear stiffness effects cause spectral peaks to broaden and flatten as well as to shift the frequency of maximum response. This discovery was unreported prior to this work. In addition, it was demonstrated that increased damping, while broadening spectral peaks in the linear stiffness range, narrows spectral peaks and reduces spectral shift where nonlinear stiffness effects are large. In addition, as nonlinear effects become more dominant, peak definition is tending to total obfuscation.

The results of this study demonstrates that nonlinear stiffness effects may play an important role in the response of composite panels even relatively low loading levels. For the panel discussed in Appendix C, the nonlinear effects are evident at 90 dB and are significant at 100 dB. Many applications currently see acoustic loading of these intensities. Consideration of nonlinear effects, therefore, may be more important than was previously considered.

Of important consequence is the fact that nonlinear stiffness effects are a significant mechanism of spectral broadening. This study demonstrates that not only are the nonlinear stiffness contributions significant but that they are coupled to the effects of linear damping. While not studied in this work, it is a logical conjecture that nonlinear damping mechanisms, if relevant will have effects which are coupled to nonlinear stiffness effects. It may be unrealistic in application, therefore, to uncouple or ignore

nonlinear effects even in relatively mild loading regimes.

For the important application of sonic fatigue life prediction, the accurate understanding of panel response is critical, but not sufficient knowledge. Just as nonlinear effects play a significant role in the response characteristics of the deformation, they may have separate and sizeable impact on fatigue life characteristics. Most fatigue damage theories in vogue either explicitly or implicitly assume the applicability of modal superposition and the validity of the Fourier transformation. This has by no means been demonstrated for the nonlinear oscillator. The results of this study demonstrate, for the white noise loading regime and the simple nonlinearity considered, that the resulting deformation process are ergodic and stationary. This does not, however, indicate that the mapping from time domain to frequency domain (and the inverse) are correct or unique. Indeed, the results for sinusoidal loading indicate that the mapping is probably not unique.

To fully understand even the single degree of freedom oscillator, significant additional research is required and must be performed in the time domain. Loading spectra other than white noise must be investigated, coupling effects between stiffness and damping mechanisms must be studied and cross correlation between field quantities (e.g. velocity and deflection) must be delineated. The current study, while yielding important insight into the problem, has just scratched the surface of understanding the response of

nonlinear oscillators subjected to random loading.

REFERENCES

1] "A Numerical Solution of Duffing's Equation Including the
    Prediction of Jump Phenomena", E.T. Moyer Jr. and E.
    Ghasghai-Abdi, AIAA Paper, AIAA-87-0917-CP, Proceedings of
    AIAA Dynamics Specialists Conference, Monterey, Calif., 1987.

2] "Time Domain Simulation of the Response of Geometrically
    Nonlinear Panels Subjected to Random Loading", E.T. Moyer,
    Proceedings of the AIAA Structures, Structural Dynamics and
    Materials Conference, AIAA, Williamsburg, Va., 1988.

3] "Sonic Fatigue Design Techniques for Advanced Composite
    Airplane Structures", I. Holehouse, AFWAL-TR-80-3019,
    Wright Patterson Air Force Base, Ohio, 1980.

4] "Sonic Fatigue Testing of an Advanced Composite Aileron",
    J. Soovre, Journal of Aircraft, Vol. 19, pp. 304, 1982.

5] "Comparison of the Statistical Properties of the Aluminum and
    CFRP Plates Subjected to Acoustic Excitation", R.G. White,
    Composites, pp. 251, 1978.

6] "Derivation and Application of the Fokker-Planck Equation to Discrete Nonlinear Dynamic Systems Subjected to White Random Excitation", T.K. Caughey, J. Acoustical Society of America, Vol. 35, pp. 1683, 1963.

7] "Nonlinear Theory of Random Vibrations", T.K. Caughey, in Advances in Applied Mechanics, Vol. 11, Academic Press, 1971.

8] "Perturbation Techniques for Random Vibration of Nonlinear Systems", S.T. Crandall, J. Acoustical Soc. of America, Vol. 35, pp. 1700, 1963.

9] "Response of a Nonlinear String to Random Excitation", R.H. Lyon, J. Acoustical Soc. of America, Vol. 32, pp. 953, 1960.

10] "Stochastic Linearization of Multi-Degree-of-Freedom Nonlinear Systems", T.S. Atlik and S. Utku, Earthquake Engineering and Structural Dynamics, Vol. 4, pp. 411, 1976.

11] "Application of Statistical Linearization to Nonlinear Multidegree of Freedom Sytems", W.D. Iwan and I.M. Yang, J. Appl. Mechanics, pp. 545, 1972.

12] "Nonlinear Panel Response by a Monte Carlo Approach" R. Vaicaitis, E.H. Dowell and C.S. Ventres, AIAA Journal, Vol. 12, pp. 685, 1974.

13] "The Response of Nonlinear Structures to Random Excitation"
C.W.S. To, Shock and Vibration, Vol. 16, pp. 13, 1984.

14] Numerical Initial-Value Problems in Ordinary Differential
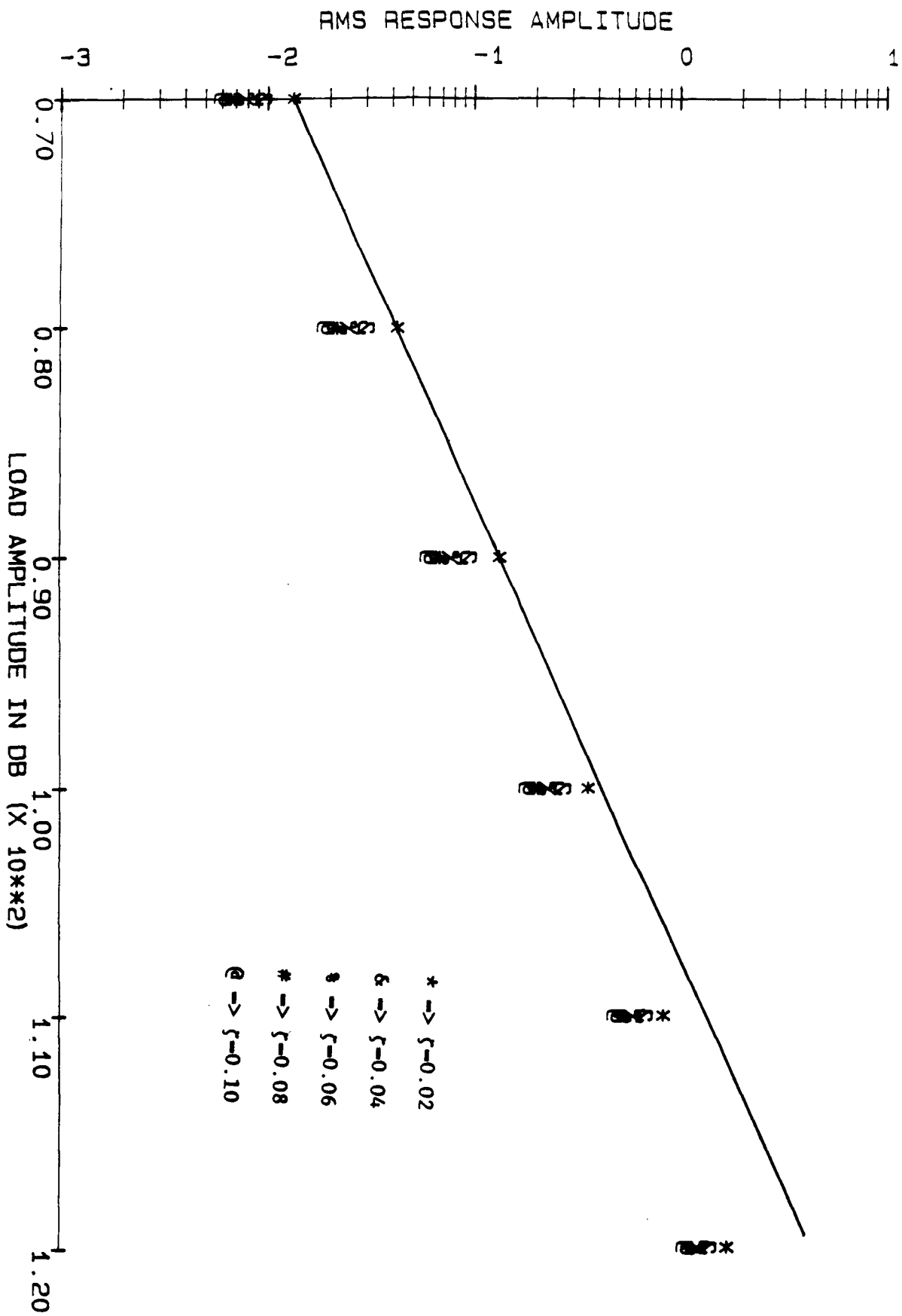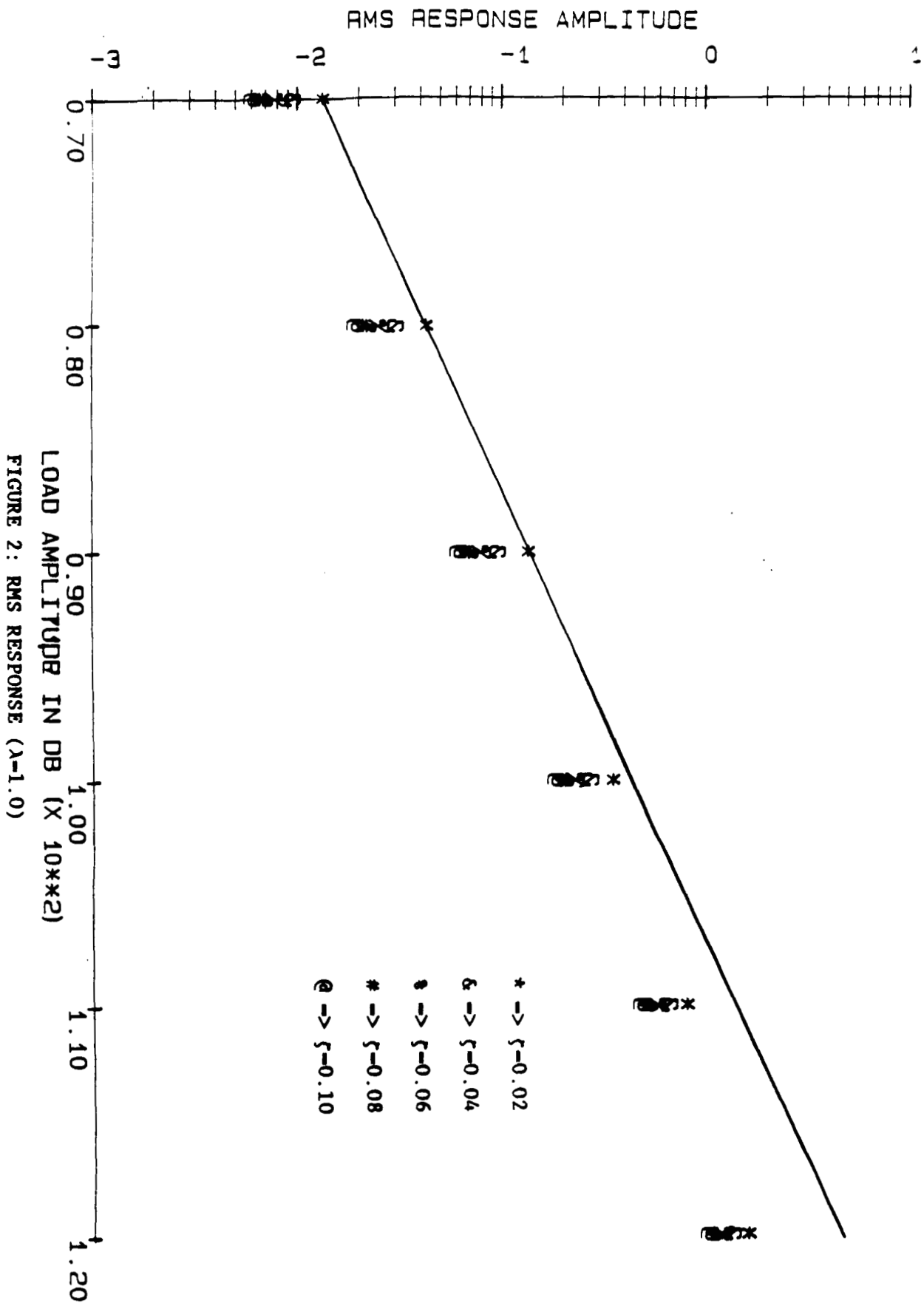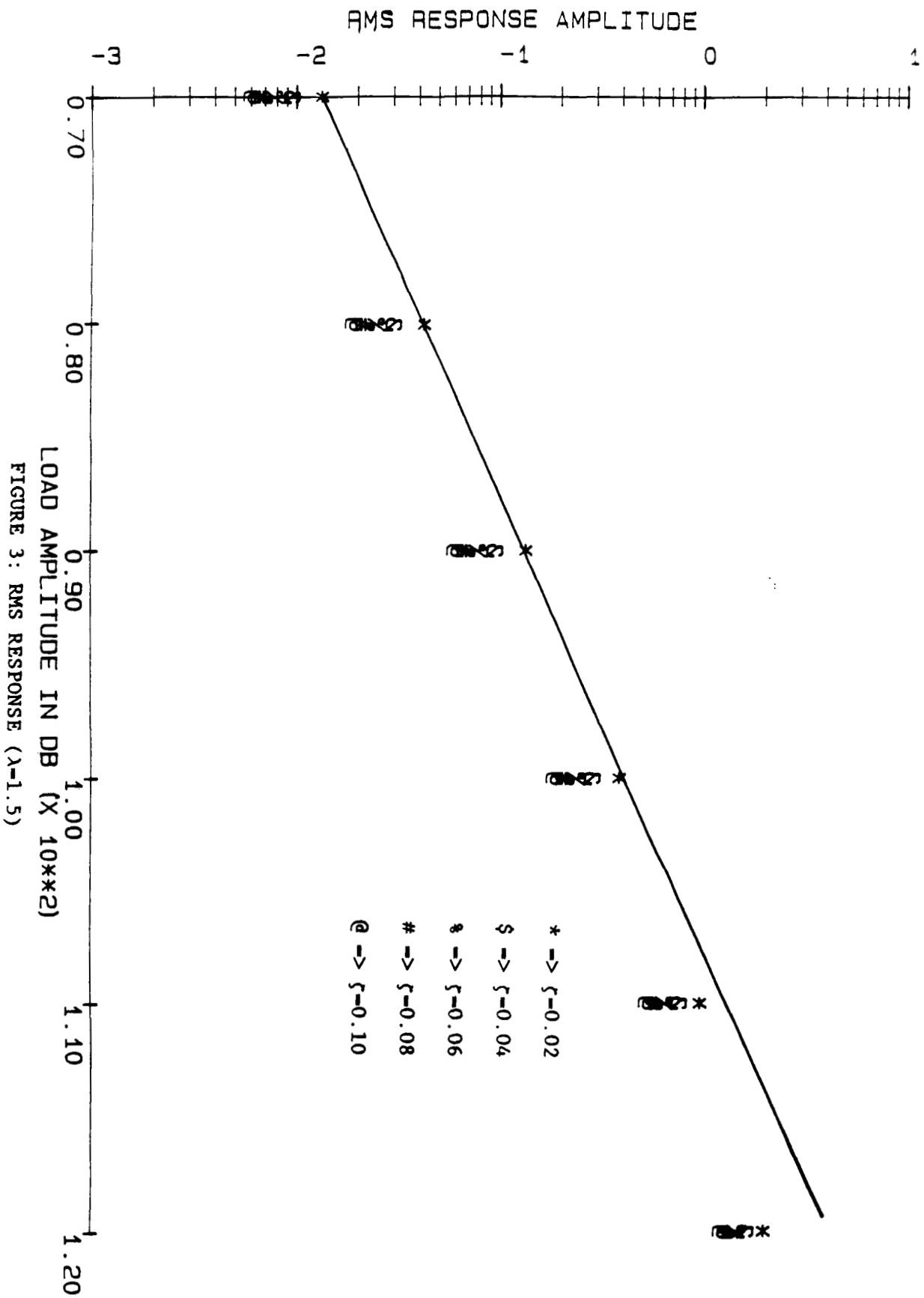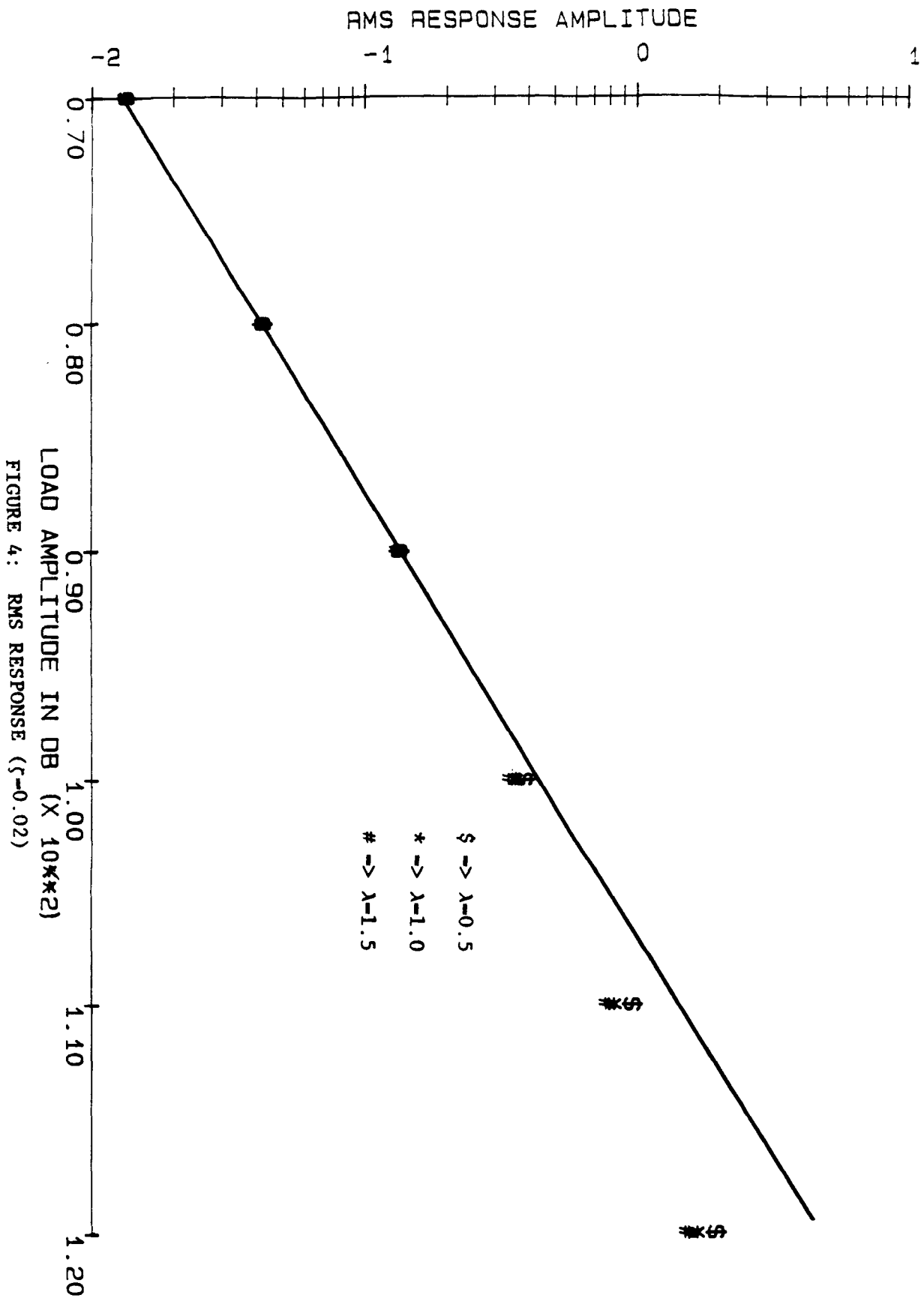Equations, C.W. Gear, Prentice-Hall, Inc., New Jersey, 1971.

FIGURE 1 : RMS RESPONSE (λ=0.5)

FIGURE 2: RMS RESPONSE (λ—1.0)

RMS RESPONSE AMPLITUDE

-3   -2   -1   0   1

0.70

0.80

0.90

1.00

1.10

1.20

LOAD AMPLITUDE IN DB (X 10**2)

* -> ζ=0.02
$ -> ζ=0.04
& -> ζ=0.06
# -> ζ=0.08
@ -> ζ=0.10

FIGURE 3: RMS RESPONSE (λ=1.5)

RMS RESPONSE AMPLITUDE

LOAD AMPLITUDE IN DB (X 10**2)

FIGURE 4: RMS RESPONSE ($\zeta=0.02$)

$ -> $\lambda=0.5$

* -> $\lambda=1.0$

-> $\lambda=1.5$

FIGURE 5: RMS RESPONSE ($\zeta = 0.06$)

RMS RESPONSE AMPLITUDE

LOAD AMPLITDUE IN DB (X 10**2)

FIGURE 6:   RMS RESPONSE (ς—0.10)

$ —> λ—0.5
* —> λ-1.0
# —> λ-1.5

RESPONSE SPECTRAL DENSITY

-10 -9 -8 -7 -6 -5 -4 -3 -2 -1

70dB
80dB
90dB
100dB
110dB
120dB

FREQUENCY IN HZ. (X 10**2)

0.00   0.50   1.00   1.50   2.00   2.50   3.00

FIGURE 7: RSD (λ-1.0; ζ-0.02)

RESPONSE SPECTRAL DENSITY

FIGURE 8: RSD ($\lambda=0.5$; $\zeta=0.02$)

FREQUENCY IN HZ. (X 10**2)

70dB
80dB
90dB
100dB
110dB
120dB

RESPONSE SPECTRAL DENSITY
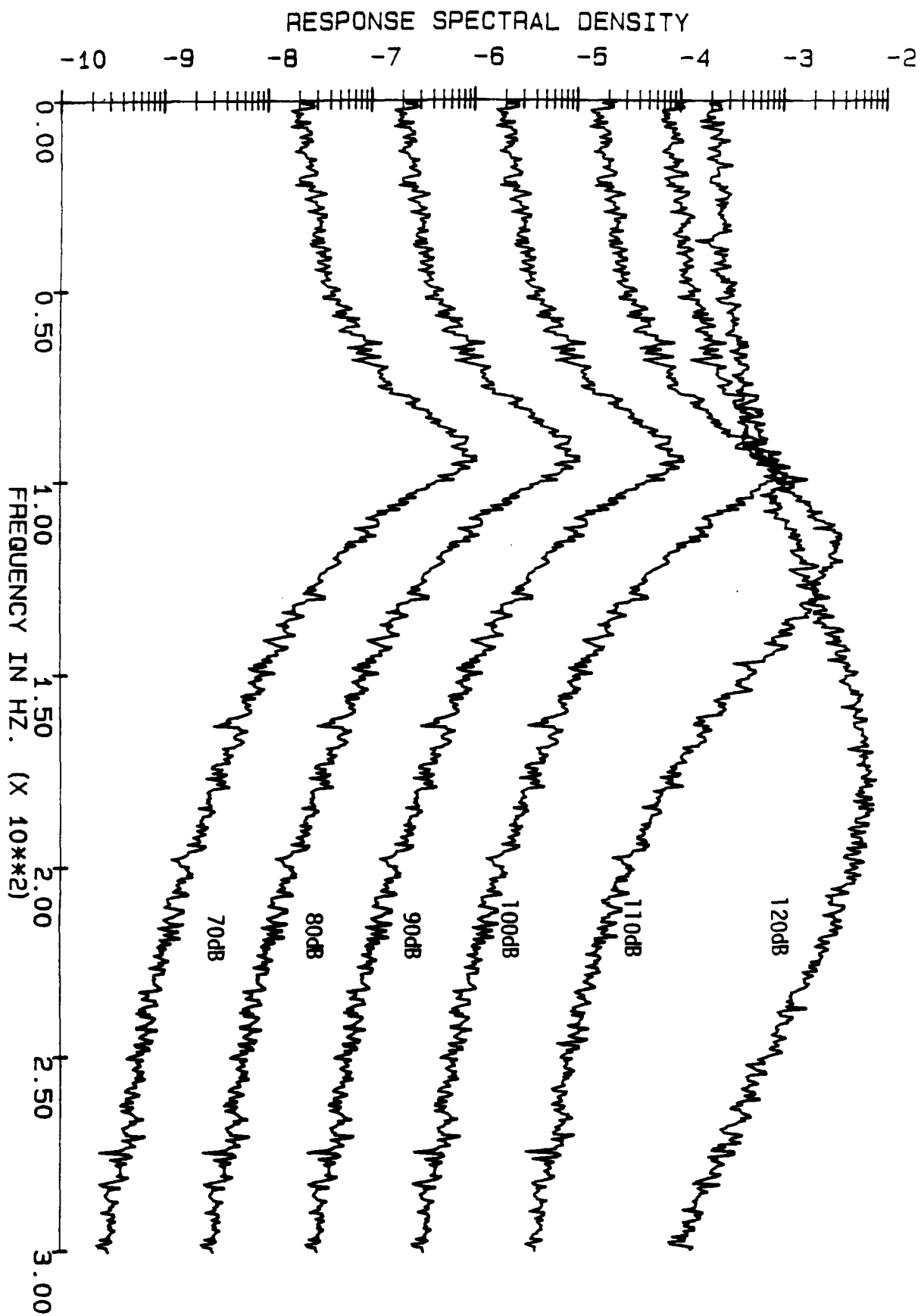
FIGURE 9: RSD (A-1.5; ζ-0.02)

RESPONSE SPECTRAL DENSITY

FIGURE 10:   RSD (λ-1.0; ζ-0.04)

RESPONSE SPECTRAL DENSITY

FIGURE 11: RSD (λ-1.0; ζ-0.06)

FREQUENCY IN HZ. (X 10**2)

70dB
80dB
90dB
100dB
110dB
120dB

RESPONSE SPECTRAL DENSITY

-10   -9   -8   -7   -6   -5   -4   -3   -2

0.00

0.50

1.00

FREQUENCY IN HZ. (X 10**2)

1.50

2.00

2.50

3.00

70dB   80dB   90dB   100dB   110dB   120dB

FIGURE 12: RSD (λ=1.0; ζ=0.08)
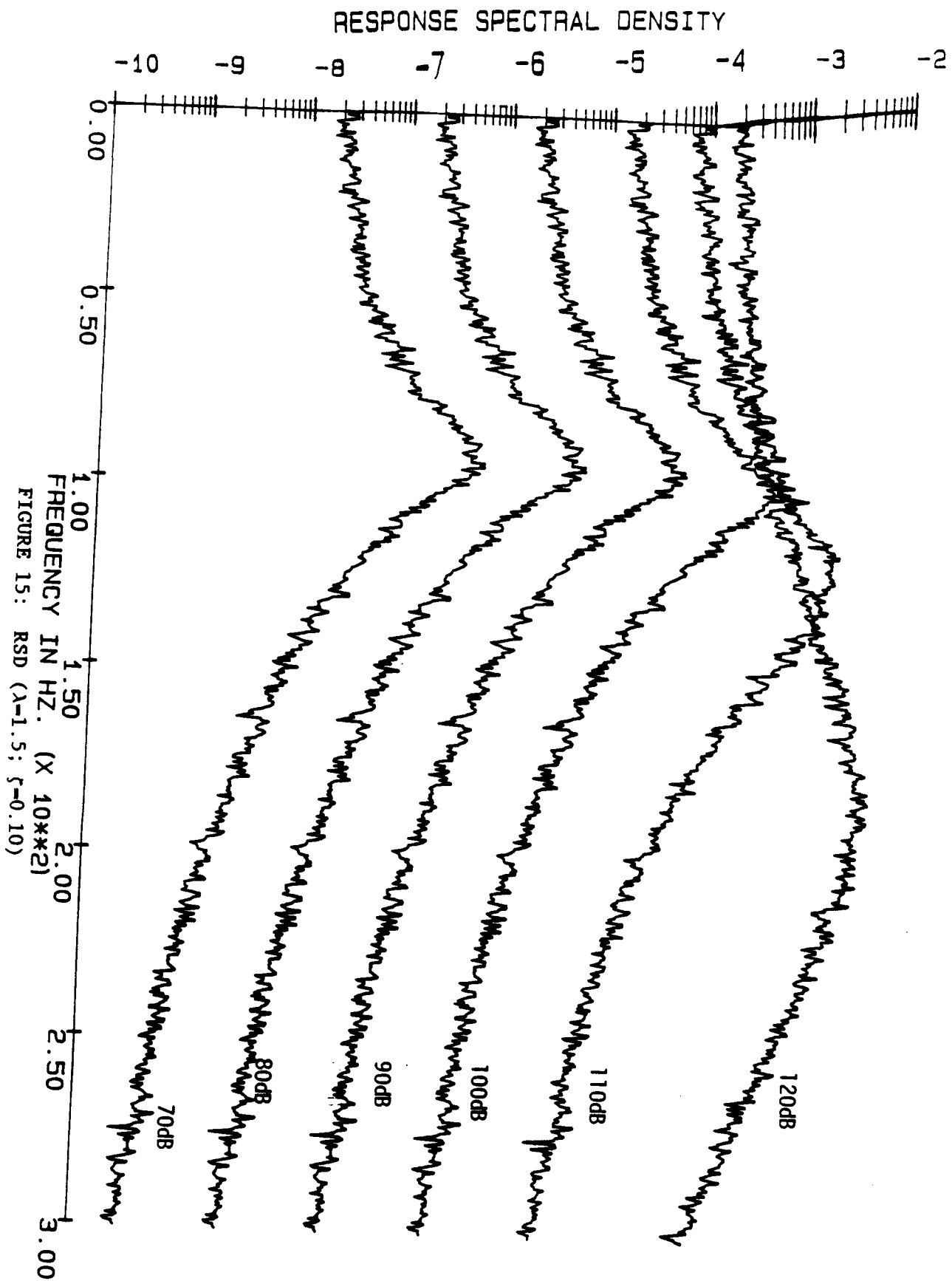
RESPONSE SPECTRAL DENSITY

-10   -9   -8   -7   -6   -5   -4   -3   -2

70dB
80dB
90dB
100dB
110dB
120dB

FREQUENCY IN HZ. (X 10**2)

FIGURE 13: RSD (λ=1.0; ς=0.10)

RESPONSE SPECTRAL DENSITY

-10   -9   -8   -7   -6   -5   -4   -3   -2   -1

0.00

0.50

1.00
FREQUENCY IN HZ. (X 10**2)

FIGURE 14: RSD (λ−0.5; ζ−0.10)

1.50

2.00

70dB

80dB

90dB

100dB

110dB

120dB

2.50

3.00

RESPONSE SPECTRAL DENSITY

FREQUENCY IN HZ. (X 10**2)

FIGURE 15: RSD (λ=1.5; ζ=0.10)

70dB
80dB
90dB
100dB
110dB
120dB

RESPONSE SPECTRAL DENSITY

FIGURE 16:   RSD (70dB; λ-1.0)

RESPONSE SPECTRAL DENSITY

FIGURE 17: RSD (80dB; λ=1.0)

RESPONSE SPECTRAL DENSITY

FIGURE 18: RSD (80dB; $\lambda = 0.5$)

RESPONSE SPECTRAL DENSITY

ζ-0.02
ζ-0.04
ζ-0.06
ζ-0.08
ζ-0.10

FREQUENCY IN HZ. (X 10**2)

FIGURE 19: RSD (80dB: λ-1.5)

RESPONSE SPECTRAL DENSITY

FIGURE 20: RSD (90dB; λ~1.0)

FREQUENCY IN HZ. (X 10**2)

RESPONSE SPECTRAL DENSITY

ζ=0.10
ζ=0.08
ζ=0.06
ζ=0.04
ζ=0.02

FREQUENCY IN HZ. (X 10**2)

FIGURE 21: RSD (100dB; λ-1.0)

RESPONSE SPECTRAL DENSITY

ζ=0.10
ζ=0.08

ζ=0.06
ζ=0.04
ζ=0.02

FREQUENCY IN HZ. (X 10**2)

FIGURE 22: RSD (110dB; λ=1.0)

RESPONSE SPECTRAL DENSITY

FREQUENCY IN HZ. (X 10**2)

FIGURE 23: RSD (110dB; λ—0.5)

RESPONSE SPECTRAL DENSITY

FIGURE 24:   RSD (110dB; λ=1.5)

RESPONSE SPECTRAL DENSITY

FREQUENCY IN HZ. (X 10**2)

FIGURE 25: RSD (120dB; λ-1.0)

RESPONSE SPECTRAL DENSITY

λ=0.5
λ=1.0
λ=1.5

FREQUENCY IN HZ. (X 10**2)

FIGURE 26: RSD (90dB; ζ=0.02)

RESPONSE SPECTRAL DENSITY

λ—0.5
λ—1.0
λ—1.5

FIGURE 27: RSD (90dB; ζ—0.06)

FREQUENCY IN HZ. (X 10**2)

RESPONSE SPECTRAL DENSITY

λ=0.5
λ=1.0
λ=1.5

FIGURE 28: RSD (90dB; ζ=0.10)

FREQUENCY IN HZ. (X 10**2)

RESPONSE SPECTRAL DENSITY

λ=1.0

λ=0.5

λ=1.5

FIGURE 29: RSD (100dB; ζ=0.06)

FREQUENCY IN HZ. (X 10**2)

RESPONSE SPECTRAL DENSITY

λ=0.5

λ=1.0

λ=1.5

FIGURE 30: RSD (100 dB; ζ=0.10)

FREQUENCY IN HZ. (X 10**2)

RESPONSE SPECTRAL DENSITY

FIGURE 31: RSD (110dB; ζ—0.02)

RESPONSE SPECTRAL DENSITY

λ-0.5
λ-1.0
λ-1.5

FREQUENCY IN HZ. (X 10**2)

FIGURE 32:   RSD (110dB; ζ-0.06)

FIGURE 33: RSD (110dB; ζ−1.0)

APPENDIX A: COMPARISON WITH EXPERIMENTS

SUMMARY OF EXPERIENCE WITH THE LANGLEY DATA

One of the original goals of this study was to compare the predicted response characteristics with tests to be performed under the direction of Mr. Carl Rucker and Dr. John Mixson at the NASA Langley research Cent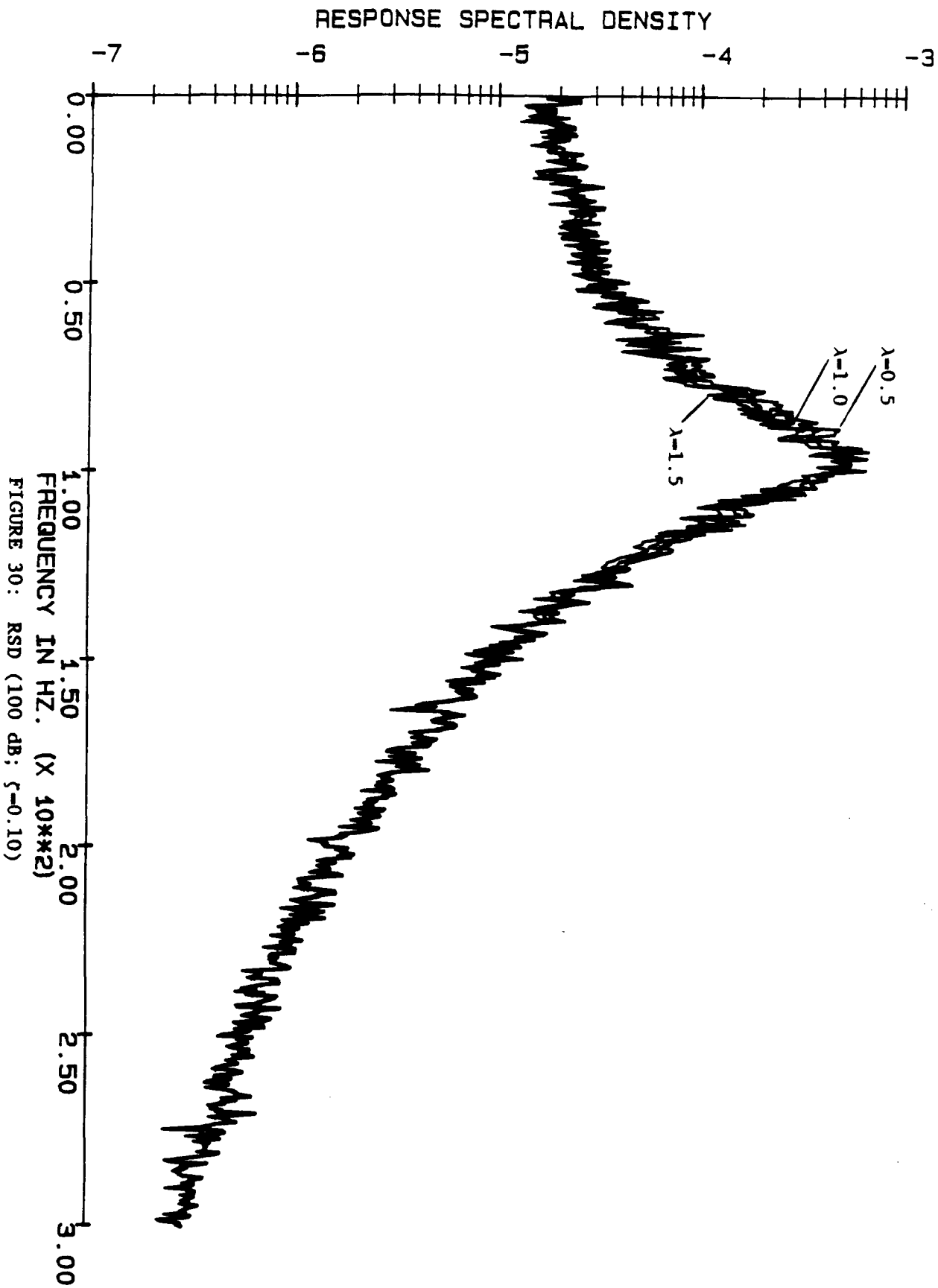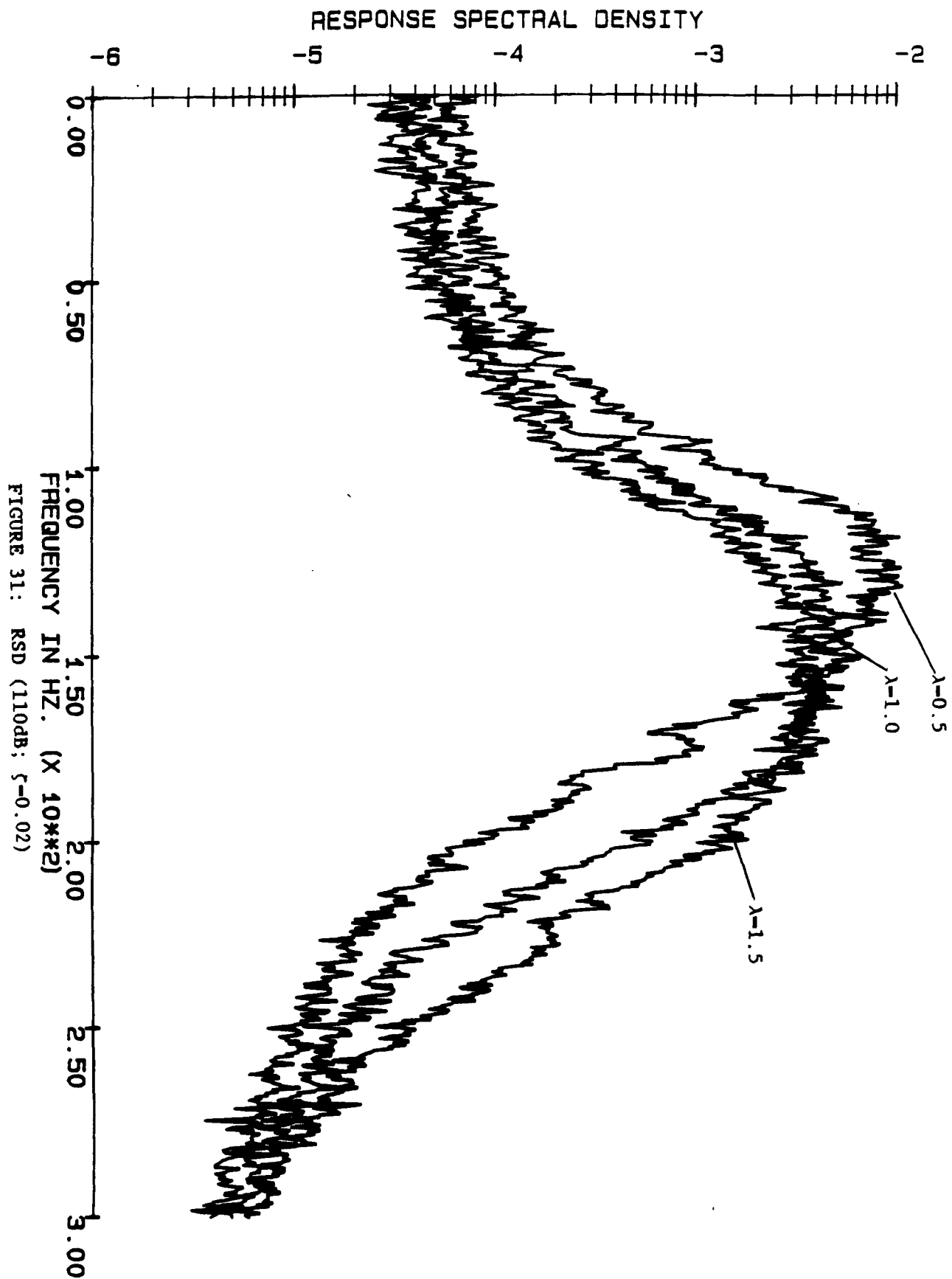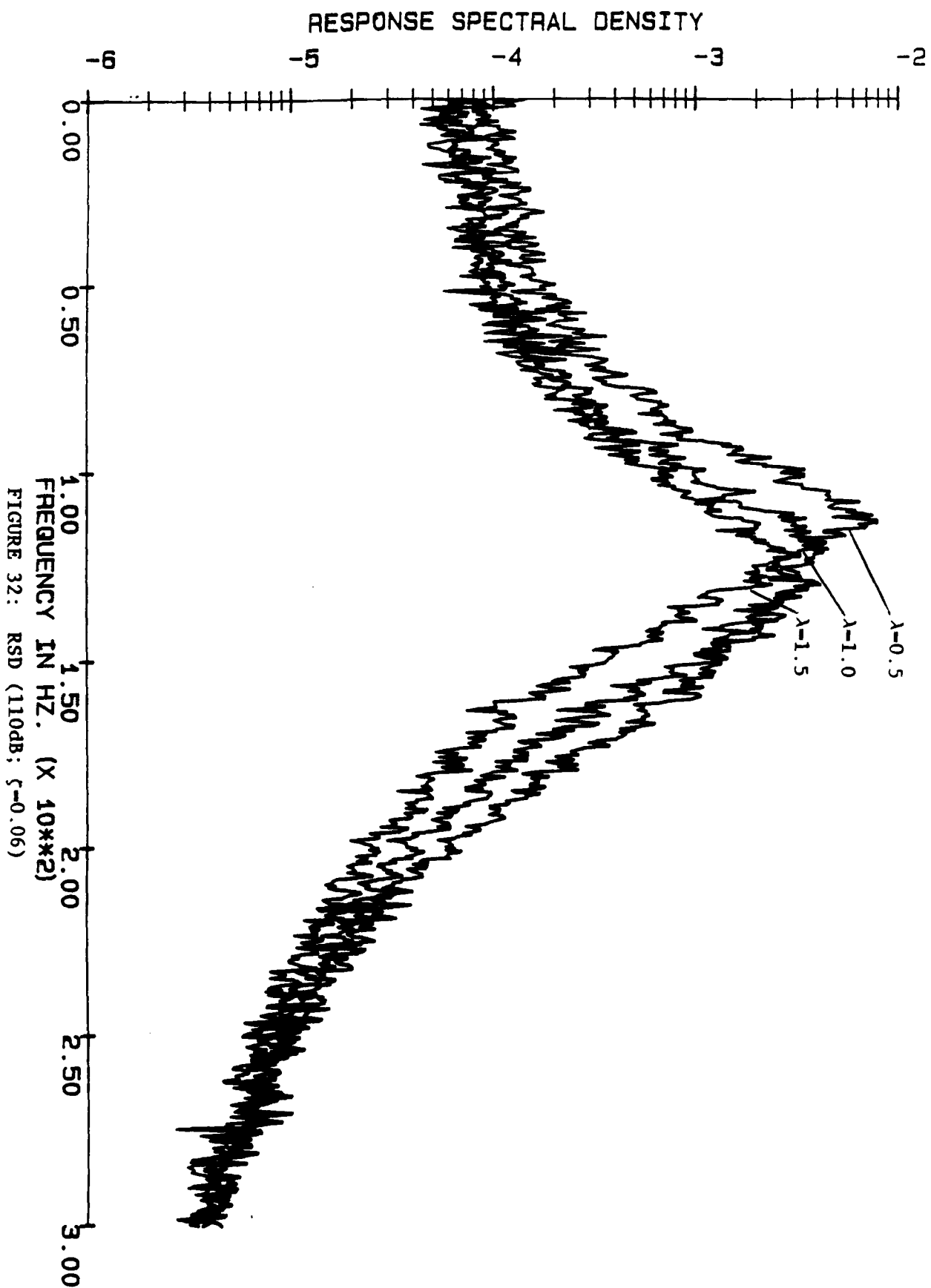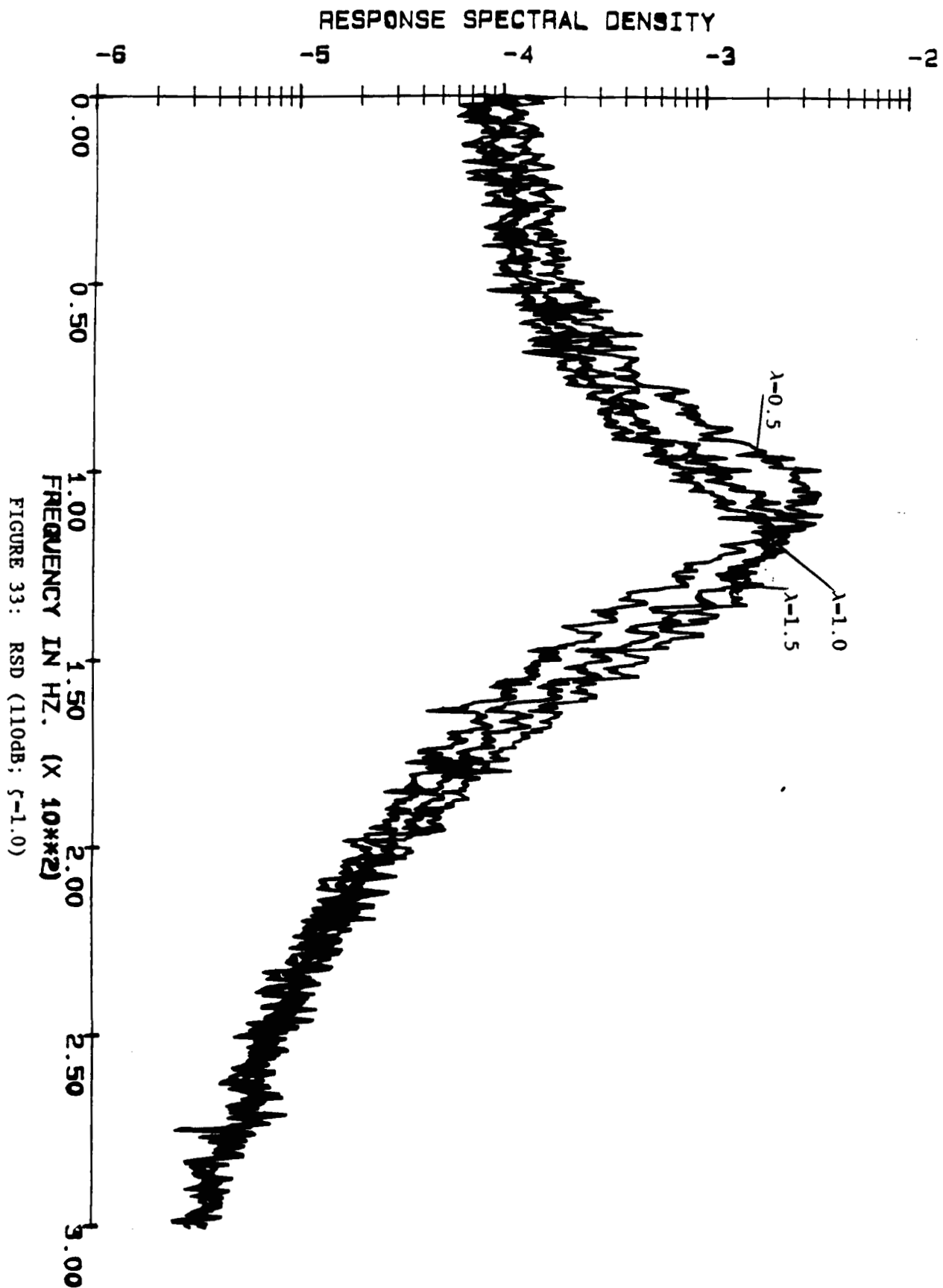er. Tests were to be run on both aluminum and graphite-epoxy panels. These panels were to be secured in a circular aperture (rigid) to insure clamped edge conditions.

Several tests were performed. The results can be obtained from Mr. Rucker. At The George Washington University, we reduced much of the data obtained. Preliminary data indicated that white noise conditions (i.e. flat loading spectra) and uniform load distribution across the panel were not well produced in the lab. In addition, the aluminum panel results indicated that the boundary conditions were not rigidly clamped edges. It also did not appear possible to drive the aluminum panel into the nonlinear region. For these reasons, a joint decision was made to not compare numerical results with the data for the aluminum panels. It was hoped the composite panels would show better boundary response and be more easily excited into the nonlinear regime.

The composite panel results demonstrated additional problems. Due to thermal conditions in the laboratory, the panel buckled and deformed during the history. This distortion manifested itself in soft spring nonlinear behavior for some test runs and hard spring on others. It was impossible to determine the appropriate

parameters for this panel even for a given test run. Modeling of initial curvature effects was beyond the scope of this study. In addition, it was not clear that the buckling was at all geometrically regular or that the boundary conditions were any closer to perfectly clamped. A final difficulty was in trying to determine an equivalent damping parameter. Repeating tests on the panel during a single day produced different results indicating a history dependence obviously absent from the analytical model. It was jointly determined that comparison with this data would not be fruitful.

In the real world, panels used in aircraft and aerospace structures are apt to demonstrate many of the same phenomena exhibited by the test panels at NASA Langley. The understanding of these effects, however, must be determined after understanding the ideal flat plate with known (if not perfectly clamped) and quantifiable damping. Response and fatigue models must be compared with a reliable data base generated from panels and loading conditions which are as close to the theoretical assumptions as possible. For understanding of composite panel response to acoustic loading and for the prediction of sonic fatigue life, significant testing is required under very basic conditions. These tests must be performed prior to the introduction of other effects (such as thermal expansion, thermal gradients, buckling and curvature effects) or it will be impossible to discern the applicability of any theoretical or numerical modeling. Correlation with this type of complicated data prior to establishing the basic theoretical

modeling will reduce to an exercise in parameter fitting which can not be extrapolated to application.

APPENDIX B:

"A Numerical Solution of Duffing's Equation
Including the Prediction of Jump Phenomena"

By: E.T. Moyer Jr. and E. Ghasghai-Abdi

Proceedings of the AIAA Dynamics Specialists Conference

Held in Monterey, California

Published by the AIAA, 1987

APPENDIX C:

"Time Domain Simulation of the Response of Geometrically
Nonlinear Panels Subjected to Random Loading"

By: E.T. Moyer Jr.

Proceedings of the AIAA Structures, Structural Dynamics
and Materials Conference

Held in Williamsburg, Va.

Published by the AIAA, 1988

APPENDIX C:

"Time Domain Simulation of the Response of Geometrically

Nonlinear Panels Subjected to Random Loading"

By: E.T. Moyer Jr.

Proceedings of the AIAA Structures, Structural Dynamics

and Materials Conference

Held in Williamsburg, Va.

Published by the AIAA, 1988

TIME DOMAIN SIMULATION OF THE RESPONSE
OF GEOMETRICALLY NONLINEAR PANELS
SUBJECTED TO RANDOM LOADING

By E. Thomas Moyer Jr.
Associate Professor of Engineering and Applied Science
Department of Civil, Mechanical and Environmental Engineering
The George Washington University
Washington, DC 20052

Abstract

The response of composite panels subjected to random pressure loads large enough to cause geometrically nonlinear responses is studied. A time domain simulation is employed to solve the equations of motion. A staged damping approach is employed to remove transients efficiently. An adaptive time stepping algorithm is employedto minimize intermittent transients. A modified algorithm for the prediction of response spectral density is presented which predicts smooth spectral peaks for discrete time histories.

Results are presented for a number of input pressure levels and damping coefficients. Response distributions are calculated and compared with the analytical solution of the Fokker-Planck equations. RMS response is reported as a function of input pressure level and damping coefficient. Spectral densities are calculated for a number of the examples. The results show excellent agreement with the Fokker-Planck solution. The RMS predictions and the predicted distributions are extremely accurate. The spectral density calculations demonstrate that the response peaks broaden as and flatten as a function of input pressure level (at a constant damping level). These results indicate that the nonlinear stiffness of the panel can account for some spectral broadening of the response.

Introduction

Over the past twenty five years, many authors have studied the problem
of obtaining an understanding of how a flexural member responds to
random, time dependent loading. If the member response is linear,
exact methodologies exist to address this problem (see, for example,
[1]). Often, however, the member exhibits nonlinear characteristics
due either to nonlinear material behavior (e.g. plasticity or
viscoplasticity) or "large" deformations. In either of these
situations, the problem becomes much more difficult.

Of interest in aerospace applications is the problem of determining
the response of flexural members subjected to random loading in the
regime where geometric nonlinearities occur. Many current and future
applications contain critical structural elements which exhibit
response magnitudes which necessitate nonlinear analysis (see, for
example, [2,3,4]). A clear understanding of the response of these
members is critical to the success and safety of current and future
aerospace vehicle design.

Several different approaches have been proposed over the years for the
analysis of nonlinear systems subjected to random time histories. The
most commonly employed methodologies are the Fokker-Planck equation
solutions [5,6], perturbation methods [7,8], stochastic linearization
techniques [9,10] and time domain methodologies (or Monte Carlo
approaches [11,12]). Each of these methods have their proponents and
have been employed for a variety of problems. Each, however, have
some inherent problems or open questions.

The Fokker-Planck equation solutions are to be employed whenever

possible as they yield exact solutions for the response probabilities and statistics. Unfortunately, the input spectra which can be analyzed is extremely limited. The solutions are best employed for comparison with approximate methodolgies as a test problem.

Perturbation approaches are employed for a wide class of nonlinear problems in mathematics and mechanics. Since a variety of techniques can be devised around the same concept it is difficult to generalize as to the range of applicability of the approach. It is fair, however, to note that the method is based on the assumption that the nonlinearity is small relative to the total characteristic of the system. This methodology, therefore, is best suited to weakly nonlinear systems.

Over the years, many methods of stochastic linearization have been suggested for the solution of nonlinear oscillator problems. In general, peak response frequencies and RMS (root mean square) response characteristics are predicted to within engineering satisfaction for moderately nonlinear systems. The methodolgy, however, has been applied to a wide variety of problems in which the response probability density function and the driving probability density function are quite different. In these problems, stochastic linearization can not yield meaningful spectral information even if the peak response frequencies and RMS values are reasonable.

Time domain simulation or Monte-Carlo approaches have been employed for the solution of nonlinear systems for many years. While the methodology is straightforward, several problems exist. For systems with small structural damping, considerable time may be required to

damp out the transients in the system. Also if the damping is light, errors in the solution can excite pseudo-transients in the response which can cause local errors in the response. In addition, depending on the time integration approach chosen and the stability limit, large numbers of time steps are often required to obtain statistically valid response distributions [13,14]. The most critical problem with time domain solutions, however, is the difficulty in extracting spectral information from discrete time histories.

In this work, a single oscillator subjected to wide band white noise is studied by time domain simulation. The Newmark time integrator is employed for reponse prediction [15]. A graded damping approach is employed which minimizes the time required to remove the transients in the system without affecting the long time response [16]. An adaptive time stepping approach is introduced which minimizes the appearance of pseudo-transients and improves the local accuracy of the solution.

A major emphasis in this work is the introduction of an improved spectral response calculation approach. The approach employs a careful blending of windowing and overlapping data segments which reduces (somewhat) computation time while producing a remarkably smooth response in the areas of interest.

The problem addressed is representative of a typical composite panel used in application. Response statistics, distribution characteristics and spectral densities are predicted. Different damping coefficients and driving force levels are studied. Comparison is made with other prediction methodologies.

Problem Description

Consider a symmetrically laminated composite plate subjected to transverse loading. If the plate deflections are assumed to be large in the von-Karmen formulation sense, the equations of motion can be written in terms of the out of plane displacement, W and a stress function F as [17]

$$\rho h \ddot{W} + L_1(W) - \phi(F,W) - P(t) = 0 \tag{1-a}$$

$$L_2(F) + 1/2 \, \phi(W,W) = 0 \tag{1-b}$$

where the differential operators are given by

$$L_1(\ ) = D_{11} \frac{\partial^4(\ )}{\partial X^4} + 4D_{16} \frac{\partial^4(\ )}{\partial X^3 \partial Y}$$

$$+ 2(D_{12} + 2D_{66}) \frac{\partial^4(\ )}{\partial X^2 \partial Y^2} \tag{2-a}$$

$$+ 4D_{26} \frac{\partial^4(\ )}{\partial X \partial Y^3} + D_{22} \frac{\partial^4(\ )}{\partial Y^4}$$

$$L_2(\ ) = A_{22} \frac{\partial^4(\ )}{\partial X^4} - 2A_{26} \frac{\partial^4(\ )}{\partial X^3 \partial Y}$$

$$+ (2A_{12} + A_{66}) \frac{\partial^4(\ )}{\partial X^2 \partial Y^2} \tag{2-b}$$

$$- 2A_{16} \frac{\partial^4(\ )}{\partial X \partial Y^3} + A_{11} \frac{\partial^4(\ )}{\partial Y^4}$$

$$\phi(V_1,V_2) = \frac{\partial^2 V_1}{\partial Y^2} \frac{\partial^2 V_2}{\partial X^2} + \frac{\partial^2 V_1}{\partial X^2} \frac{\partial^2 V_2}{\partial Y^2}$$

$$- 2 \ \frac{\partial^2 v_1}{\partial X \partial Y} \frac{\partial^2 v_2}{\partial X \partial Y} \qquad\qquad (2\text{-}c)$$

In this formulation, the plate is assumed to be thin and the in-plane and rotary inertia contributions have been ignored. The matrix components Aij and Dij are dependent only on the material constants. If a single space mode for the out of plane displacement, W, is assumed to be in the form

$$W = \frac{\psi(t)h}{4} \ (1 + \cos \frac{2\pi X}{a}) \ (1 + \cos \frac{2\pi Y}{b}) \qquad\qquad (3)$$

and the stress function, F, is defined accordingly, the equation of motion can be reduced to the form

$$\ddot{\psi} + 2\zeta\omega_o\dot{\psi} + \omega_o^2\psi + \beta\psi^3 = \frac{p(t)}{m} \qquad\qquad (4)$$

where ω_o is the linear angular frequency, β is the nonlinear stiffness, ζ is the damping coefficient, m is the total plate mass and P(t) is the loading pressure as a function of time. The parameters are calculated for a clamped, rectangular panel with uniform pressure loading in the transverse direction. The assumed material properties are

$$
\begin{aligned}
E_1 &= 23.7 \times 10^6 \ \text{PSI} \\
E_2 &= 1.48 \times 10^6 \ \text{PSI} \\
\sigma_{12} &= 0.94 \times 10^6 \ \text{PSI} \\
\gamma_{12} &= 0.30 \\
\rho &= 1.459 \times 10^{-4} \ \text{LB} - \text{SEC}^2/\text{IN}^4
\end{aligned}
\qquad\qquad (5)
$$

and the plate dimension are

$$a = 15 \text{ inches} \quad -\frac{a}{2} \leq X \leq \frac{a}{2}$$

$$b = 12 \text{ inches} \quad -\frac{b}{2} \leq Y \leq \frac{b}{2} \tag{6}$$

$$h = 0.04 \text{ inches}$$

The problem described corresponds to a typical composite panel used in application. The damping coefficient is varied in the analysis as most application have uncertain damping characteristics. The problem described has previously been studied by Mei and Prasad using stochastic linearization [18]. Details of the formulation can be found in that paper.

The loading function, P(t) is assumed to be wide band white noise. A standard Gaussian white noise generator was implemented [19] to produce a flat spectral density. Since a discrete time domain solution can only simulate band limited white noise, numerical experimentation was employed to determine suitable cutoff frequencies. Cutoff frequencies from 10 to 100 times the linear resonance frequency were tested. Response statistics were stable for all cutoff frequencies studied. Unfortunately, the spectral estimates were quite sensitive to cutoff frequency as is well documented. To minimize the cutoff frequency effect, all responses employed a cutoff frequency of 10,000 hz. For practical applications, a lower cutoff frequency could probably have been employed, however, spectral calculations may show more "noise" as discussed subsequently.

The Fokker-Planck equations provide an exact solution for this problem [6]. For the general oscillator of the form

$$\ddot{X} + \beta\dot{X} + F(X) = f(t) \tag{7}$$

where

$$F(X) = \omega_o^2 [X + \epsilon g(X)] \qquad (8)$$

The response distribution function is given as

$$P(X) = C \exp\left[\frac{1}{\sigma_{\dot{x}}^2} \left[\frac{x^2}{2} + \epsilon G(X) \right] \right] \qquad (9)$$

where

$$G(X) = \int_o^X g(\sigma)d\sigma \qquad (10)$$

For the problem of equation 5, therefore, the distribution is

$$P(\psi) = C \exp\left[\lambda_1(\frac{\psi^2}{2} + \lambda_2\psi^4) \right] \qquad (11)$$

$$C, \lambda_1, \lambda_2 \rightarrow \text{constant}$$

This will be compared with the time domain solution to demonstrate the accuracy of the response.

Time Integration Approach

To integrate the equation of motion (equation 5), the Newmark time integrator [15] was employed. For the problem in this paper, the algorithm takes the form

$$\dot{\psi}^{n+1} = \dot{\psi}^n + \frac{\Delta t}{2} \left[F(\psi^{n+1}, \dot{\psi}^{n+1}) - F(\psi^n, \dot{\psi}^n) \right]$$

$$\psi^{n+1} = \psi^n + \Delta t\, \dot{\psi}^n + \frac{\Delta t^2}{4} \left[F(\psi^{n+1}, \dot{\psi}^{n+1}) - F(\psi^n, \dot{\psi}^n) \right]$$

$$F(\psi, \dot{\psi}) = \frac{p(t)}{m} - 2\varsigma\omega_0\dot{\psi} - \omega_o^2\psi - \beta\psi^3 \qquad (12)$$

where Δt is the time step size. This integrator is unconditionally stable for the linear oscillator ($\beta = 0$). For the nonlinear oscillator, however, no stability analysis has been performed to date. Experience has shown, however, that accuracy is the limiting concern for the Newmark integrator for practical problems [16].

The input load is calculated at a discrete number of points determined by the cutoff frequency. The data point spacing is given by

$$\Delta\tau = \frac{T_o}{100}$$
$$\qquad (13)$$
$$T_o = \frac{2\pi}{\omega_o}$$

To solve the equation of motion, therefore, this is the largest time step permissable. In practice, choosing the time of equation 11 will yield a solution with intermittent transients. Numerical experimentation demonstrated that the time step required to solve the equation of motion without encountering intermittent transients was on the order of

$$\Delta t = \frac{\Delta\tau}{12} \qquad (14)$$

for the most severe case studied. To produce a statistically significant number of points, however, would have required a large number of time steps. To reduce this requirement, an adaptive technique was introduced. Assume the solution is known at a time T with corresponding driving function Q(T). It is desired to proceed

from T to T + $\Delta\tau$ in M equal time steps. The driving function at T + $\Delta\tau$ is given as Q(T+ $\Delta\tau$). If Qmax and Qmin are the maximum and minimum values the driving function exhibit, the number of time steps is chosen as

$$M = 2 + 10 * \frac{Q(T + \Delta\tau) - Q(T)}{Q_{max} - Q_{min}} \qquad (15)$$

This worked well for all problems studied. The choice of the multiplicative factor in equation 13 should, however, be a function of the damping coefficient and the driving function level instead of being held constant. Since this was chosen for the most severe case, the results should be good for all cases. More work could lead to an optimization of this approach, however.

In the time domain solution approach, damping is required to produce a steady state solution. While it can be argued that damping will be exhibited by any real structure, that damping is often light. To remove the transients from the system may require significant amounts of computation. To accelerate removal of the transients, a staged approach was employed. To start the solution, initial response and velocity was assumed to be zero. The damping coefficient was multiplied by 1000 and the solution was generated for 100 * $\Delta\tau$. The damping was then abruptly reduced to 100 times the true damping level and the solution was continued for 100 * $\Delta\tau$. The damping was again dropped to 10 times the true damping and the solution continued for an additional 100 * $\Delta\tau$. The damping was then set to the true (physical level). The solution was then continued for the desired length of time. RMS statistics were accumulated dynamically. When both response and velocity values remained constant for time segments

of 100 times the linear period, the solution was considered to be in steady state. The response was then generated to the desired stopping point. This was achieved in under 50,000 * $\Delta\tau$ for all problems studied.

After steady state was achieved, the solution was generated for 1,000,000 * $\Delta\tau$. Samples were taken in $\Delta\tau$ increments. These points were then used to calculate response statistics and distributions. Part of this time trace was also used to calculate response spectral density. The approach described is by no means optimized. Currently (as described), the parameters are all based on numerical experiment. Those employed in this study, however, produce very accurate responses with no detectable intermittent transients. The cumulative response statistics vary by less than 0.1% over the total time history. This methodology could be studied parametrically to determine general forms for the parameters involved.

Spectral Density Estimation

A response measure which often yields important information in the study of random vibrations is the Spectral Density (often called the Power Spectral Density, PSD). The PSD is defined as the normalized Fourier Transform of the autocorrelation function. The autocorrelation function is defined by

$$R_\psi(t) = \int_{-\infty}^{\infty} \psi(\tau+t)\psi(\tau)\frac{d\tau}{T} \tag{16}$$

and is related to the PSD by

$$2\pi S_\psi(\omega) = \int_{-\infty}^{\infty} R_\psi(\tau)e^{-i\omega\tau}d\tau \tag{17}$$

Using the theory of Fast Fourier Transforms (FFTs), the PSD can be estimated $N/2+1$ discrete frequencies equally divided between 0 and the cutoff (or Nydquist) frequency by the formulae [20].

$$S_\psi(f=0) = \frac{1}{N^2} |C_\phi|^2$$

$$S_\psi(f=f_k) = \frac{1}{N^2} [|C_k^2| + |C_{N-k}|^2] \qquad (18)$$

$$k=1,\ldots,N/2-1$$

$$S_\psi(f=f_o) = \frac{1}{N^2} |C_{N/2}|^2$$

for a sample of N discrete data c which are c^j related to the C_k by the formulae

$$C_k = \sum_{j=0}^{N-1} c_j \, e^{2\pi i j k/N} \qquad k=0,\ldots,N-1 \qquad (19)$$

In practice, this approach leads to much "leakage" which can be solved by windowing the data or using a weighted approach to minimize the leakage. The algorithm is then modified to

$$S_\psi(0) = \frac{|D_o|^2}{W_{ss}}$$

$$S_\psi(f_k) = \frac{1}{W_{ss}} [|D_k|^2 + |D_{N-k}|^2] \qquad (20)$$

$$k=1,\ldots,N/2-1$$

$$S_\psi(f_c) = \frac{1}{W_{ss}} |D_{n/2}|^2$$

where

$$D_K = \sum_{j=0}^{N-1} C_j W_j e^{2\pi i j k/N} \qquad k=0,\ldots n-1$$

$$W_{ss} = N \sum_{j=0}^{N} W_j^2 \qquad\qquad (21)$$

The window function , w_j is chosen to minimize leakage and to have the properties of being 0 at the ends of the data segment, 1 at the center and be monotonic between the ends and the center. Generally, windows are positive definite functions. The choice of a window function, however, is quite arbitrary. In this work, the Parzen window has been chosen as it is a consistently good performing function for discrete oscillator systems [21]. The Parzen window is given by the formula

$$W_j = 1 - \left| \frac{j-(N-1)/2}{(N+1)/2} \right| \qquad\qquad (22)$$

For N discrete data points separated by the time increment appropriate for the chosen Nydquist frequency, the algorithm presented will yield an estimate of the PSD at N/2+1 discrete frequencies. This approach, however, yields estimates with horrendous variance for most realistic applications.

To minimize the variance at the discrete estimate frequencies, an alternative scheme can be employed. The available data can be broken into segments. Each segment can be employed to calculate a PSD estimate at M discrete frequencies where 2*M is the segment length.

The estimates can then be averaged to produce a smoother PSD estimate than if data had been used as previously described. If the total number of segments sampled is K, then, a total of 2KM points are used. It can be shown that this reduces the variance by a factor of K [22]. An improvement to this approach involves using overlapping data segments. If the total available data is partitioned in samples of length M and if K segments are considered, each of length 2M, the segment data is chosen such that the segments overlap. In the standard approach, the first and second sample make up the first segment, the second and third sample make up the second segment, etc. This reduces the variance by a factor of approximately 9K/11 for a total sample of (K+1)M points [22].

For the problem studied in this work, the PSD results showed large variance (on the order of 100%) for the linear oscillator using the overlapping segment approach (other methods were worse). This is consistent with other investigator's observations [23]. To improve the PSD estimation, a different overlapping approach was employed. The total sample was divided into samples of length J. The first segment employed 4 samples: J=1, J=2, J=3 and J=4. The second segment employed samples: J=2, J=3, J=4, and J=5, etc. For a total of K segments, (K+3)*J points were employed. Typical runs for the linear oscillator using a Nydquist frequency of 10 times the resonance frequency and on the order of 200,000 points, the observed variance was reduced to less than 20% in the region near the peak. Specific results will be discussed in the next section.

The approach described above was implemented on an Alliant FX8/2 computer. Typical runtimes were on the order of one CPU minute for

200,000 data points. Many numerical experiments were performed both on the linear oscillator system and band limited white noise. In general, the algorithm performed very consistently over a wide range of input signals. Maximum variances were kept below 20% in regions of interest and spurious peaks were not observed. White noise results were excellent with typical tails on the order of 5% of the Nydquist frequency. For a fixed number of data points, the algorithm employing three overlapping samples produced significantly better estimates for the mean squared response compared with the single overlap algorithm (calculated as the discrete integral of the PSD using Simpson's 3/8 rule). For single degree of freedom oscillators, a prescribed variance tolerance could be met with significantly fewer data points using three overlapping segments making this approach computationally more attractive. In practice, small tolerances could not be met using the single overlap algorithm.

Results

The plate described in equations (4,5,6) was studied for many input amplitudes and damping coefficients. Figure 1 is a plot of the RMS response amplitude

$$\psi_{RMS}^2 = \sum_{j=1}^{N} \frac{\psi_1^2}{(N-1)} \tag{23}$$

as a function of the driving Sound Spectrum Level (SSL) for damping coefficients corresponding to 1%, 2%, 4%, 6%, 8% and 10% critical (i.e. ς = 0.01 , 0.02 , 0.04 , 0.06 , 0.08 , 0.10). The straight line represents the results from the linear theory with ς=0.01 . As is well known, the response predicted by the linear theory is greater than that predicted by the nonlinear theory for a given damping coefficient. In addition, the increase in damping causes a decrease

in the RMS response as is expected. The prediction are in good agreement with the predictions using the Method of Equivalent Linearization (MEL) reported by Mei and Prasad [18]. Maximum difference between the two methods was 4%.

To further investigate the accuracy of the results obtained by time domain simulation, the probability density function was calculated from the response sample. The range of responses ($-3 < \psi < 3$) was divided into 200 bins equally distributed. The histogram was then integrated and normalized numerically so the total probability integral equaled 1. The points at the center of each bin where then plotted and connected. A total of 1,000,000 sample points were employed. The results are shown in Figure 2 for an input SSL of 110 DB and a damping coefficient of ζ -0.01. In addition, the exact distribution of equation 9 is plotted along with the predicted Gaussian response of the MEL. The results from the time domain simulation are in remarkable agreement with the exact solution as is shown. The Gaussian prediction, however, is quite different. The MEL predictions heavily weight the response toward the zero mean and overestimate the tail distribution. The time domain results, in contrast, accurately predict the broader and flatter distribution of the exact solution. The exact solution is modeled quite well over the whole distribution range, including the tails.

Of major interest was the prediction of the response PSD using the algorithm described previously. Figure 3 shows the predicted linear oscillator PSD for a panel with a damping coefficient of 1% critical and a driving input SSL of 70 DB. The response should be a linear damped oscillator respone with exact solution in the form

$$S_\psi(f) = \frac{S_I}{(\omega^2 - \omega_o^2)^2 + 4\varsigma^2 \omega^2 \omega_o^2} \tag{24}$$

.

$$\omega = 2\pi f$$

where S_I is the input spectral density corresponding to 70 DB SSL. The predicted PSD is in good agreement with the exact solution for the range plotted. The PSD varies by almost three orders of magnitude in the range studied near the peak. The response PSD peak and shape are well predicted. As will be discussed subsequently, PSD tails tend to be over predicted and quite noisy. For physical interest, however, this is not of major consequence since this happens when PSD values are several orders of magnitude below peak values.

Of interest is the effect of increasing driving SSL on the response PSD. The MEL results of Mei and Prasad indicated that increasing SSL did not effect the spectral characteristics of the oscillator. MEL predicts a shift in the resonance frequency and in the magnitude of the PSD, but not in the width or shape of the distribution. Figure 4 shows the PSD from the time domain simulation and from the MEL for a driving SSL of 110 DB with 1% critical damping. The two methods predict quite different response PSDs. The time domain results demonstrate significant broadening and flattening of the spectral density. The characteristic linear oscillator sharp peak is no longer evident. The MEL results predict the expected linear sharp peak. The MEL results predict a much larger peak value also. It is important to notice that the PSD predictions from the time domain simulation show relatively small variances and consistent response patterns. The difference between the two methods does not appear to be due to the

numerical approach employed.

Figure 5 is a plot of the response PSD for the nonlinear oscillator with 1% critical damping at 80, 90, 100 and 110 DB SSL driving levels. The 80 DB results are fairly linear in form with a resonance frequency of around 94 hz. (the linear resonance frequency is 92.9 hz.). At 90 DB, the PSD results have shifted slightly (peak response is now around 100 hz.) and the peak has broadened slightly. At 100 DB, a larger shift is observed and the response has broadened and flattened considerably. A discernable resonance peak is no longer observable. As previously discussed, at 110 DB significant broadening and flattening has taken place. All results in this figure are for a constant damping ratio ($\zeta=0.01$). The PSD results generally are considered by the author to be accurate. It is important to mention, however, that the tails may be overestimated. Studies with linear oscillators (with known exact solutions) demonstrated overestimation of tail predictions but only when the response was several orders of magnitude less than the peak.

Also of interest is the effect of damping on the predicted response PSDs. Figure 6 is a plot of the predicted response PSDs at 1%, 2%, 4%, 6% and 10% critical damping coefficients. As is expected from the linear theory, the peaks diminish and flatten with increasing damping (linear, viscous, damping only is considered in this study). Damping only effects the peak responses and the tails are insensitive to damping as expected from the linear theory. It is evident from Figure 1 that at 80 DB SSL, the system should behave linearly. This is confirmed.

Figure 7 is a plot of the predicted response PSDs at 1%, 2%, 4%, 6% and 10% critical damping coefficients. In contrast to the linear oscillator, the increase in damping decreases the spectral width and sharpens the response PSD. The high frequency side of the PSD is effected much more than the lower frequency side. The frequency at maximum PSD moves back toward the linear resonance frequency, in effect, linearizing the system. This is not totally unexpected. At higher damping ratios, the RMS response is lowered, lowering the effects on nonlinearity. At 10% critical damping and 110 DB SSL, the RMS amplitude is about equal to the RMS amplitude for 1% critical damping at 100 DB. The predicted peak frequencies are about the same and the predicted maximum PSD values are similar.

Discussion and Conclusions

The results presented demonstrate that the time domain simulation (or Monte Carlo) approach provides an accurate numerical methodology for the study on nonlinear oscillators. Not only are qualitative predictions possible but the exact probability density and response statistics are reproducible. The method, therefore, should provide a quantitatively accurate tool for studying nonlinear phenomena in other loading regimes (i.e. for more complicated loading spectra than white noise).

Methodology for the prediction of response PSDs was briefly reviewed. A new (to the author's knowledge) overlapping scheme is employed which reduces prediction variance significantly (but in a quantitatively unknown amount). The results are in good agreement with the exact results for linear oscillators. Quantitatively accurate estimates have been obtained for several problems with known spectral densities.

With the exception of tail regions or within 5- 10% of the Nydquist frequency, the results are believed to be accurate for a wide variety of problems.

The spectral density results as a function of increasing SSL were studied. At higher SSL, the nonlinearity manifests itself by broadening and flattening the PSDs. The resonance frequency (or peak frequency) is shifted to higher levels and the broadening is skewed to the high frequency side. The drop off is faster for the high frequency tail and the response is not symmetric about the resonance frequency. It is interesting to note that the RMS response for a sinusoidally driven oscillator qualitatively demonstrates the same behavior due to hard spring nonlinearities. The resonance peak is shifted to higher frequency, the peak is broadened and bent to the high frequency side. The broadening and flattening of spectral peaks due to hard spring nonlinearity, therefore, may not be totally surprising.

The response results have been compared with those predicted by the MEL. MEL predictions agree in RMS responses. PSD predictions, however, are quite different. Resonance frequencies (or frequencies at peak PSD) are roughly the same, however, at 110 DB, the PSD predictions show such a broad resonance that the concept may not be applicable. It is not surprising that the RMS response predictions are in good agreement as the MEL is based on minimizing the error of

the RMS predictions. The inherent assumption of a Gaussian response, however, is clearly incorrect for large SSL as indicated in Figure 2. This may explain the large difference in PSD predictions between the two methods. Since the time domain simulation agrees with the exact probability density extremely well, the PSD predictions from the time domain are expected to be more reliable than the MEL predictions.

Increased viscous damping has a linearizing effect on a nonlinear oscillator. Since the RMS response is decreased, the nonlinear term decreases in importance causing the system to be more linearly. For the 110 DB SSL results (shown in Figure 7), the PSD peak is narrowed and shifted back toward the linear resonance frequency at higher damping ratios. For a linear oscillator, the PSD peak is broadened for increasing damping. This broadening, however, is small relative to the broadening due to the nonlinear stiffness effects. The broadening due to damping, therefore, will probably only be evident when the nonlinearity is small or negligeable.

The results of this study indicate that considerable spectral broadening can be attributed to nonlinear stiffness effects alone. This may be of significant importance in the prediction of sonic fatigue failures. Spectral broadening (and increased probability of higher amplitude oscillations) is indicative of a wider peak distribution. Sonic fatigue predictions are based on the concept of acumulated damage which is a function of the weighted average of the instantaneous (or discrete peak) responses. The effect of hard spring nonlinearity, therefore, may be more critical than indicated by a particular RMS response level.

Acknowledgements

References

[1] Newland, D.E., An Introduction to Random Vibrations and Spectral Analysis, Longman Group, ltd., Essex, England, 1984.

[2] Holehouse, I., "Sonic Fatigue Design Techniques for Advanced Composite Airplane Structures", AFWAL-TR-80-3019, Wright Patterson Air Force Base, Ohio, 1980.

[3] Soovere, J., "Sonic Fatigue Testing of an Advanced Composite Aileron", Journal of Aircraft, Vol. 19, pp. 304-310, 1982.

[4] White, R.G., "Comparison of the Statistical Properties of the Aluminum and CFRP Plates Subjected to Acoustic Excitation", Composites, 1978, pp. 251-258.

[5] Caughey, T.K., "Derivation and Application of the Fokker-Planck Equation to Discrete Nonlinear Dynamic Systems Subjected to White Random Excitation", Journal of the Acoustical Society of America, Vol. 35, 11963, pp. 1683-1692.

[6] Caughey, T.K., "Nonlinar Theory of Random Vibrations", in Advances in Applied Mechanics, Vol. 11, Academic Press, 1971.

[7] Lyon, R.H. "Response of a Nonlinear String to Random Excitation", Journal of the Acoustical Society of America, Vol. 32, 1960, pp. 953-960.

[8] Crandall, S.T., "Perturbation Techniques for Random Vibration of Nonlinear Systems", Journal of the Acoustical Society of America, Vol. 35, 1963, pp. 1700-1705.

[9] Iwan, W.D. and Yang, I.M., "Application of Statistical Linearization to Nonlinear Multidegree-of-Freedom Systems", Journal of Applied Mechanics, June, 1972, pp. 545-550.

[10] Atalik, T.S. and Utku, S., "Stochastic Linearization of Multi-Degree-of-Freedom Nonlinear Systems", Earthquake Engineering and Structural Dynanmics, Vol. 4, 1976, pp. 411-420.

[11] Dowell, E.H., "Nonlinear Oscillation of a Fluttering Plate I", AIAA Journal, Vol. 4, 1966, pp. 1267-1275.

[12] Vaicaitis, R., Dowell, E.H. and Ventres, C.S., "Nonlinear Panel Response by a Monte Carlo Approach", AIAA Journal, Vol. 12, 1974, pp. 685-691.

[13] To, C.W.S., "The Response of Nonlinear Structures to Random

Excitation", Shock and Vibration, Vol. 16, 1984, pp. 13-33.

[14] Crandall, S.H. and Zhu, W.Q., Random Vibration: A Survey of Recent Developments", Journal of Applied Mechanics, Vol. 50, 1983, pp. 953-962.

[15] Bathe, K.J. and Wilson E.L., Numerical Methods in Finite Element Analysis. Prentice-Hall Publishing Company, New Jersey, 1976.

[16] Moyer, E.T.,Jr., and Ghasghai-Abdi, E., "A Numerical Solution of Duffing's Equation Including The Prediction of Jump Phenomena", AIAA Dynamics Specialists Conference, Monterey, Calif., 1987.

[17] Chia, C.Y., Nonlinear Analysis of Plates. McGraw-Hill, 1980.

]18] Mei, C. and Prasad, C.B., "Response of Symmetric Rectangular Composite Laminates with Nonlinear Damping Subjected to Acoustic Loading", Proceedings of the 10th AIAA Aeroacoustics Conference, Seattle, Wash., 1986.

[19] Shinozuka, M. and Jan, D.M., "Digital Simulation of Random Processes and Its Applications", Journal of Sound and Vibration, Vol. 25, 1972, pp. 111-128.

[20] Press, W.H., Flannery, B.P., Teukolsky, S.A., Vetterling, W.T., Numerical Recipes. Cambridge University Press, Cambridge, England, 1986.

[21] Priestlley, M.B., Spectral Analysis and Time Series. Academic Press, 1981.

[22] Childers, D.G. Modern Spectrum Analysis. IEEE Press, New York, 1978.

[23] Beauchamp, K.G. and Yuen, C.K., Digital Methods for Signal Analysis. George Allend and Unwin, London, 1979.